Received: 18 January 2023 | Accepted: 31 August 2023

DOI: 10.1002/jpln.202300020

RESEARCH ARTICLE

Synergistic relationships between the age of soil organic matter, Fe speciation, and aggregate stability in an arable Luvisol

Nina Siebers[1] | Eva Voggenreiter[2] | Prachi Joshi[2] | Janet Rethemeyer[3] | Liming Wang[1]

[1]Institute of Bio- and Geosciences–Agrosphere (IBG-3), Forschungszentrum Jülich, Jülich, Germany

[2]Geomicrobiology, Department of Geosciences, University of Tübingen, Tübingen, Germany

[3]Institute of Geology and Mineralogy, University of Cologne, Cologne, Germany

Correspondence
Nina Siebers, Institute of Bio- and Geosciences—Agrosphere (IBG-3), Forschungszentrum Jülich, 52425 Jülich, Germany.
Email: n.siebers@fz-juelich.de

This article has been edited by Kai Uwe Totsche.

Abstract

Background: Knowledge of soil aggregate formation and stability is essential, as this is important for maintaining soil functions.

Aims: This study aimed to investigate the influence of organic matter (OM), the content of pedogenic iron (Fe) (oxyhydr)oxides, and aggregate size on the stability of aggregates in arable soil.

Methods: To this end, the Ap and Bt horizons of a Luvisol were sampled after 14 years of bare fallow, and the results were compared with a control field that had been permanently cropped.

Results: In the Ap horizon, bare fallow decreased the median diameter of the 53–250 µm size fraction by 26%. Simultaneously, the mass of the 20–53 µm size fraction increased by 65%, indicating reduced stability—particularly of larger soil microaggregates—due to the lack of input of fresh OM. The range of ^{14}carbon (^{14}C) fraction of modern C (F^{14}C) under bare fallow was between 0.50 and 0.90, and thus lower than the cropped site (F^{14}C between 0.75 and 1.01), which is particularly pronounced in the smallest size fraction, indicating the presence of older C. This higher stability and the reduced C turnover in <20 µm aggregates is probably also due to having the highest content of poorly crystalline Fe (oxy)hydroxides, compared to the other size fractions, which act as a cementing agent. Colloid transport from the Ap to the Bt horizon was observed under bare fallow treatment.

Conclusions: The lack of input of OM decreased the stability of microaggregates and led to a release of mobile colloids, the transport of which can initiate elemental fluxes with as-yet unknown environmental consequences.

KEYWORDS

^{14}C dating, occluded microaggregates, organic matter depletion, particle size distribution, subsoil

1 | INTRODUCTION

The ecosystem services of soil include nutrient cycling, water storage, carbon (C) storage, and microbial habitats, which are intimately linked to the basic heterogeneous arrangement of soil aggregates and internal pores (Bauke et al., 2022; Totsche et al., 2018). The development of a soil aggregate structure by pedogenesis is a desirable soil characteristic for sustaining agricultural production and maintaining environmental quality (Amézketa, 1999). The formation and stability of soil aggregates were therefore investigated in depth in this study. Soil aggregation is assumed to follow a hierarchical order with particles below 2 µm acting as the smallest building units. These micro-structured basic units are essentially made up of clay minerals, pedogenic oxides, and organic matter (OM) that adhere together and form organo-mineral associations (Kögel-Knabner et al., 2008; Lehmann et al., 2007). The smallest building units combined form soil microaggregates, which in turn are subunits of macroaggregates. The boundary dividing microaggregates and macroaggregates has been widely accepted to be 250 µm (Six et al., 2004; Tisdall & Oades, 1982; Totsche et al., 2018). The assembly of differently sized aggregates forms a three-dimensional structure with connected voids and dead voids as well as pores of different shapes, sizes, and geometries. This continuous network of the pore system is a dynamic biogeochemical interface, as it facilitates the flow of gases and water. The architecture and stability of the aggregates, that is, their function of providing niches for water storage and microbial nutrient metabolism, strongly depend on the spatial organization of the individual building units, their specific elemental composition, and the spatial distribution of metal oxides (cementing agents) and OM (gluing agents; Totsche et al., 2010, 2018). Stable aggregates are therefore beneficial in soil for many reasons, including C sequestration, nutrient retention, aeration, and erosion control as well as providing microenvironments for soil microorganisms.

The hierarchical nature of aggregated soil implies that different aggregation mechanisms may apply for different sizes of aggregates. There is evidence that the stability of aggregates correlates inversely with size (Golchin et al., 1994; Krause et al., 2018; Siebers et al., 2018; Six et al., 2002). For small microaggregates (<20 µm), the binding forces predominantly seem to be short-range van der Waals forces and electrostatic binding, which are strong enough to withstand disintegration by ultrasound treatment (M. Kaiser & Berhe, 2014; M. Kaiser et al., 2012). Not only are electrostatic binding and van der Waals forces important for the formation of small (i.e., <50 µm) microaggregates, but polysaccharides and microbial-derived OM were also highly relevant in gluing microaggregates. However, for the formation of larger microaggregates, fresh OM (i.e., plant-derived residues, partly decomposed) as a gluing agent and more crystalline iron (Fe) (oxyhydr)oxides as cementing agents are more essential to glue together building units composed of smaller microaggregates (Totsche et al., 2018). Our hypothesis, therefore, is (1) that a lack of OM input mainly affects the stability of larger soil microaggregate size fractions.

Poorly crystalline Fe (oxyhydr)oxides can be present as nanoparticles that are as small as 2 to 5 nm and as Fe (oxyhydr)oxides associated with clay minerals (X. Jiang et al., 2015; Regelink et al., 2014). During further soil development, Fe (oxyhydr)oxides are slowly transformed to more crystalline Fe (oxyhdr)oxide minerals that are less reactive, such as crystalline goethite and hematite (Cornell & Schwertmann, 2003), which are then predominantly found in the larger size fractions (Barberis et al., 1991). Goethite is the most common Fe (oxyhydr)oxide in temperate soil due to its high thermodynamic stability. Its size ranges between 5 and 100 nm, and it is positively charged in most soils due to the point of zero charge at approximately pH 8. Colloidal goethite thus actively promotes the stabilization of larger soil microaggregates (Schwertmann & Carlson, 2005) due to interactions with negatively charged clay minerals or soil OM (SOM; Kretzschmar & Sticher, 1997; Tombácz et al., 2004). Fe mineralogy therefore influences the structure, and in particular the stability, of microaggregates.

Of particular significance to the formation of microaggregates are associations built by the interaction of minerals with OM (Totsche et al., 2018). It is widely accepted that OM associations with Fe (oxyhydr)oxides lead to reduced OM turnover as shown by a positive correlation between Fe (oxyhydr)oxide and organic C (OC) content and an inverse correlation between OC turnover and Fe (oxy)hydroxide content (K. Kaiser & Guggenberger, 2000; Torn et al., 1997; Wagai & Mayer, 2007). Crystalline Fe (oxyhydr)oxides are often related to reduced SOM protection (Torn et al., 1997) relative to less-crystalline forms. The continuum of Fe-crystallinity also correlates with surface area. On one end of the continuum are poorly crystalline minerals that are represented broadly by ferrihydrite. This may also include ferric (oxyhydr)oxide minerals that are precipitated in the presence of OM (ThomasArrigo et al., 2018, and references therein). Lepidocrocite, akaganeite, goethite, magnetite, and hematite are progressively more crystalline (in that order).

The soil fraction <20 µm is involved in the protection of SOM from decomposer organisms (Lopez-Sangil & Rovira, 2013). Mechanisms for OC stabilization are occlusion within aggregates, adsorption processes, coprecipitation, or organo-Fe complexes (Eusterhues et al., 2003; Kiem & Kögel-Knabner, 2002; Moni et al., 2010; Tombácz et al., 2004; Wagai & Mayer, 2007) that can occur simultaneously along a continuum. Occluded and older OC particularly correlate to soil aggregate stability (Golchin et al., 1994). In a recent study, it was shown that with increasing OC age, the contribution of metal oxides as cementing agents increased in high-density and sonication-resistant aggregates that are mainly associated with old OC. However, plant-derived young C at a low decomposition stage acted as a gluing agent for the stabilization of low-density fractions at higher hierarchy levels and the contribution of reactive metal phases decreased (Wagai et al., 2018). We therefore assume that (2) with a lack of OM input, the content of C decreases and the relative abundance of aged OM with a narrow C/N ratio as a gluing agent increases, especially for small soil microaggregates. However, OM is not only stabilized by Fe (oxyhydr)oxides: It is also known that the interaction of short-range-ordered Fe minerals (e.g., ferrihydrite) with specific functional groups of OC inhibits crystallization to more crystalline forms such as goethite and hematite (Chen et al., 2015; Jones et al., 2009; Vodyanitskii & Shoba, 2016) due to the sorption of organic anions and, therefore, the prevention of nucleation (Cornell & Schwertmann, 1979). Our hypothesis is thus that (3) the contribution of poorly crystalline Fe (oxyhydr)oxides as a cementing agent decreases due to the decrease of OC

content under bare fallow, particularly for small microaggregate size fractions.

To test these hypotheses, we analyzed an arable Luvisol under conventional management and 14 years of bare fallow, obtained samples from the Ap and the Bt horizons, size fractionated the soil to the different soil microaggregate size fractions obtained, and analyzed the size fractions in terms of C content and age, Fe speciation, and aggregate stability.

2 | MATERIALS AND METHODS

2.1 | Study site and sampling

The study site in Selhausen (50°52'08'' N, 6°26'59' E) is part of the Lower Rhine Embayment (Germany), an intensively used agricultural area. The mean annual temperature and precipitation are 9.8°C and 694 mm, respectively. Two parallel fields are included: one field that has been under bare fallow (1.1 ha) since 2005 with the regular application of herbicides and shallow tillage (5 cm deep, once a year in 2006–2010, followed by once every 4 years); the other control field (0.5 ha) in the immediate vicinity has been permanently cropped (mainly sugar beet and winter wheat) for a century including mechanical tillage every year, that is, bare fallow versus cropped treatment. The site is characterized by a weak inclination of 1.7° in the east-to-west direction (Meyer et al., 2017; Schweizer et al., 2024). Across the slope, the soil properties are highly heterogeneous in terms of stone content with a gradient of high, medium, and low fine earth (FE) content (Meyer et al., 2017). Across the inclination, fluvial deposits of Pleistocene gravel dominate the upslope soils east of the site with lower proportions of FE, whereas Aeolian Pleistocene Loess sediments dominate the downslope soils in the west with a higher FE content. Samples were taken from the high FE content downslope, and the soil at this position was classified as Stagnic Luvisol with a silt loam texture (WRB, 2007) derived from loess mixed with fluvial deposits. In November 2019, Ap (approximately 0–32 cm) and Bt (approximately 32–52/74 cm) soil horizons were sampled from the lower slope of the cropped and bare fallow fields. The soil took the form of samples from soil pits from the Ap and Bt horizons. According to the pedogenetic features, the Ap horizon was approximately 0–31 cm, of which the material 5–25 cm was sampled with three field replicates per treatment that were kept separately for analyses unless stated otherwise. The fresh soils were sealed in plastic bags and stored in a cool chamber at 5°C until wet sieving, which was conducted no later than 3 weeks after sampling.

2.2 | Wet sieving and density separation

Wet sieving followed a modified procedure based on a previous paper (Krause et al., 2018). In brief, a sieve tower composed of three sieves (mesh size: 2800, 250, and 53 µm) was submerged into 12 L of deionized water. The water content of each individual soil sample was determined by drying the soil at 105°C until constant weight and recording the mass before and after drying. The water content was in a range of 15.0%–17.5%. Approximately 58–59 g of field-moist samples, corresponding to 50 ± 1 g dry weight, were weighed on a filter paper and pre-wetted for 5 min on the topmost 2800 µm sieve. The sieve tower was then moved up and down 30 cycles per min by an electric motor for 10 min. The >250 µm size fractions were subjected to ultrasound treatment applying an energy of 60 J mL^{-1} to release occluded soil microaggregates. The resultant suspension was sieved again to obtain 53–250 µm and 20–53 µm occluded soil microaggregates. Only the occluded size fraction was used for further analyses, as only occluded aggregates contribute to the hierarchical structure of aggregate formation. The occluded <20 µm suspension was centrifuged (Heraeus MULTIFUGE 4KR, Thermo Scientific) to separate 0.30–20 µm soil microaggregates, and <0.30 µm colloids remained in the supernatant.

Density separation was performed to remove non-aggregated primary and secondary mineral particles (Virto et al., 2008). The size fractions obtained from the wet sieving were dispersed in a sodium metatungstate solution (2.5 g cm^{-3}) and centrifuged. Only free primary and secondary particles, the density of which was assumed to be 2.65 g cm^{-3}, could be centrifuged to the bottom. The OM-associated mineral particles remained in the supernatant and were washed with deionized water and then freeze-dried for subsequent analyses, that is, elemental composition, C and nitrogen (N) analyses, ^{14}C dating, Mössbauer spectroscopy, and oxalate and dithionite-citrate-bicarbonate extractable Fe (Fe_{DCB}). A summary of which analyses were performed with which size fractions is presented in Table S1.

2.3 | Size distribution and stability test

The field fresh bulk soil (sieved to <2 mm) and the three size fractions, that is, <20, 20–53, and 53–250 µm, were freshly analyzed (directly after wet soil fractionation without prior drying) by the laser diffraction particle analyzer (Horiba LA960). To ensure homogeneity, the samples were continuously stirred and circulated to the flow cell for detection as described in Tang et al. (2022). Results of particle analysis using laser diffraction are given as a volume-based median diameter (Dv50) in µm, with the diameter of half of detected particles being above this value and the diameter of another half below this value.

We also used the particle analyzer to test for soil aggregate stability according to Mason et al. (2011). In brief, aggregates were subjected to a constant and continuous mechanical force while being stirred and circulated. Through repeated measurements of the particle size distribution over a total time of 40 min, it was possible to derive the stability of the aggregates. Within the first 10 min, we performed a measurement every 40 s, while for the last 30 min measurements were conducted every 3 min. The particle sizes obtained were evaluated for the shift in Dv50.

2.4 | Asymmetric flow field-flow fractionation (AF^4) of colloids

The elemental content of soil colloids <0.30 µm was analyzed by applying AF^4 (AF2000, Postnova Analytics) as described in Krause et al.

(2020). The OC content in the colloidal size fractions was measured using AF^4 coupled to a UV-vis detector with an absorption wavelength of 254 nm (Postnova Analytics) and to an OC detector (DOC-Labor GmbH). The element content of Fe, Al, silicon (Si), and calcium (Ca) was determined by AF^4 coupled to an inductively coupled plasma mass spectrometer (ICP-MS; Agilent 7500, Agilent Technologies) using post-channel calibration with Rh as the internal standard (Nischwitz et al., 2016). In brief, we used 25 µM L^{-1} of sodium chloride carrier solution, a 0.5 mm spacer, and a 1 kDa polyether sulfone membrane. Two milliliter of supernatant containing <0.30 µm colloids were directly injected and then focused for 12 min by 2.7 mL of flow focusing. The elution program started with 2.5 mL min^{-1} cross flow, which then decreased to 0.15 mL in 30 min and finally remained at 0 mL min^{-1} for 50 min. The results are presented as a bulk colloid fraction and not size-separated further.

2.5 | Elemental composition

Soil C and N analyses were performed using the dry combustion method followed by thermal conductivity detection of the released trace gases (vario MICRO cube, Elementar). To remove inorganic C before analysis, samples were treated with 4 M HCl for 4 h at room temperature and dried at 60°C for 16 h (ISO, 1995). The aqua regia-extractable elements (Fe, Al, Si, and Ca) of the bulk soil and size fractions, that is, <20, 20–53, and 53–250 µm, from Ap and Bt were determined after the microwave-assisted digestion of 150 mg with 0.7 mL HNO_3 and 2 mL HCl using ICP-optical emission spectrometry (Thermo Fisher iCAP 7600).

2.6 | ^{14}C analysis

The ^{14}C analyses were performed on dry bulk and size-fractionated samples (<20 and 20–53 µm). The size fraction 53–250 µm could not be analyzed, as sample amounts were not sufficient for analysis. For the other size fractions, composite samples on a weight basis of all three replicates were used to ensure a sufficient sample amount. All samples were extracted with 10%–20% HCl (1 h at 60°C plus 10 h at room temperature) depending on the inorganic C content of the sample to remove inorganic C. The acid was removed by repeated washing with ultra-pure water. After drying, the samples were converted to elemental C using an automated graphitization system (Ionplus AG), and the content of ^{14}C was measured using the University of Cologne's accelerator mass spectrometry (AMS) system. For further details, see Rethemeyer et al. (2019). The ^{14}C content was expressed as fraction modern C ($F^{14}C$; Reimer et al., 2004).

2.7 | Oxalate and Fe_{DCB}

The Fe_{DCB} was assessed by using a method according to Kiem and Kögel-Knabner (2002). This extraction targets the specific Fe (oxyhydr)oxides: ferrihydrite, lepidocrocite, akaganeite, goethite, and to a small extent hematite (Voelz et al., 2019). About 50 mg of the sample was shaken with a mixture of 0.3 M sodium citrate solution, 1.0 M sodium hydrogen carbonate, and sodium dithionite for 16 h at room temperature. After shaking and subsequent centrifugation (10 min at 3000 × *g*), the supernatant was removed, and the residue was mixed with 0.05 M $MgSO_4$. After mixing and subsequent centrifugation (10 min at 3000 × *g*), the supernatant was combined with the supernatant from the first extraction step.

The oxalate extractable Fe (Fe_{OX}) was performed with 0.2 M oxalate (mixing 0.113 M NH_4 oxalate and a 0.087 M oxalic acid solution) at pH 3.0 and 2 h shaking in the dark (Kiem & Kögel-Knabner, 2002; Schwertmann, 1964). Due to the low pH, the OH-groups on the Fe (oxyhdr)oxide surfaces are protonated, thus weakening the Fe–O bond. As a result, the oxalate ligand is able to finally dissolve the Fe (oxyhdr)oxide (Cornell & Schwertmann, 2003). The results of oxalate and DCB extraction must always be considered with reservations since not all Fe (oxyhydr)oxides are dissolved in the DCB extraction and therefore only a "pseudo-total" of Fe oxide content is determined. Oxalic acid extractions are more specific than the DCB extractions. Specifically, oxalic acid extractions target short-range order (SRO) phases: ferrihydrite and ferrihydrite-like poorly crystalline Fe (oxyhydr)oxide phases, in addition to magnetite. Since preliminary Mössbauer analyses did not show any indications of magnetite, we take the oxalate-extractable fraction to represent poorly crystalline Fe (oxyhydr)oxides including ferrihydrite. After shaking and subsequent centrifugation (10 min at 3000 × *g*), the concentration of extracted Fe was determined by ICP-MS after appropriate dilution. All bulk soil samples were analyzed in triplicate, measuring the replicates individually, while for size fractions, one composite sample (mass basis) was used due to the limited sample material.

2.8 | Mössbauer spectroscopy

Dried soil powders of the size fraction <20 µm were analyzed using Mössbauer spectroscopy, as this size fraction exhibited sufficient Fe content and is mainly involved in the protection of SOM (Lopez-Sangil & Rovira, 2013). The samples were loaded into Plexiglas holders (area 1 cm^2), forming a thin disc. The holders were inserted into a closed-cycle exchange gas cryostat (Janis cryogenics) under a backflow of He to minimize exposure to air. Spectra were collected at 5 and 77 K using a constant acceleration drive system (WissEL) in transmission mode with a $^{57}Co/Rh$ source. All spectra were calibrated against a 7-µm-thick α–5^7Fe foil that was measured at room temperature. The analysis was performed using Recoil (University of Ottawa) and the extended Voigt-based fitting routine (Lagarec & Rancourt, 1998). The half width at half maximum was limited to 0.151 mm s^{-1} during fitting. Based on the spectra collected at two temperatures (77 and 5 K, Figure S1, Table S3), we determined the fraction of Fe that was bound in (1) crystalline mineral phases such as goethite and hematite as evidenced by the sextets in the 77 K spectra; (2) poorly crystalline or short-range-ordered mineral phases such as ferrihydrite and lepidocrocite as evidenced by the sextets in the 5 K spectra that were absent in the 77 K spectra; and (3) clay minerals such as phyllosilicates as evidenced by the doublets at 77 and 5 K (Murad & Cashion, 2011). We note that the poorly

crystalline phases may also contain ferric hydroxide that has formed in the presence of OM, sometimes referred to as organo-mineral composites in which the binding environment of Fe atoms resembles that of ferrihydrite (Eusterhues et al., 2008; ThomasArrigo et al., 2018).

2.9 | Statistical analyses

Statistical analyses were performed in Excel (Excel 2016, Microsoft Corporation) using XLSTAT 2021.5 (Addinsoft). To investigate the effect of bare fallow on the median diameter, the mass of size fractions, and the median diameter determined by the stability test, we performed a Wilcoxon rank-sum test ($p < 0.05$) for each size fraction, each horizon, and each time point separately. We tested the elemental composition and Fe_{OX} and Fe_{DCB} for normal distribution using the Shapiro–Wilk test ($p < 0.05$) and for homogeneity of variances using the Brown–Forsythe test ($\alpha = 0.05$). The differences between treatments and horizons were determined by means of a one-way ANOVA ($\alpha = 0.05$). If significant differences occurred, we used the Tukey honestly significant difference (HSD) test to perform a post hoc separation of means ($\alpha = 0.05$). Due to constraints in the sample amounts, we used composite samples (weight basis) of the three replicates for ^{14}C analyses, Mössbauer spectroscopy, and oxalate and DCB extraction of size fractions, which means that a statistical evaluation is not possible.

3 | RESULTS

3.1 | Size and mass distribution of soil microaggregates

As expected, the median diameter (Dv50) of the size fractions decreased in the order 53–250, 20–53, and <20 µm independent of the horizon or the treatment. The Dv50 of the bulk soil was comparable to the 20–53 µm size fraction. A significant treatment effect was visible for the Ap 53–250 µm, Bt bulk, and Bt 53–250 µm size fractions, with significantly lower Dv50 under bare fallow (Figure 1). The reduction in the mean diameter under bare fallow for the size fraction 53–250 µm was not visible. However, there was a significant increase of the 20–53 µm mass for the Ap horizon under bare fallow, compared to the cropped site. For Bt, the partially significant (20–53 and <20 µm) reduction in Dv50 under bare fallow was also visible, with a significant reduction of the mass of the size fractions 20–53 and <20 µm, compared to the cropped site (Figure 2).

3.2 | Stability test

For all treatments and horizons, the Dv50 decreased rapidly during the first 10 min, while the reduction was always greater for Ap, compared to Bt, and for bare fallow, compared to the cropped site (Figure 3). After 19 min, the Dv50 was significantly smaller for the bare fallow Ap, compared to the cropped site Ap, and after 30 min, it was significantly smaller for the bare fallow Bt, compared to the Bt of the cropped site. After 24 min, the mean diameter remained constant or began to increase again for the Ap and Bt of the cropped site, indicating a degree of reaggregation, while this effect was not visible under bare fallow.

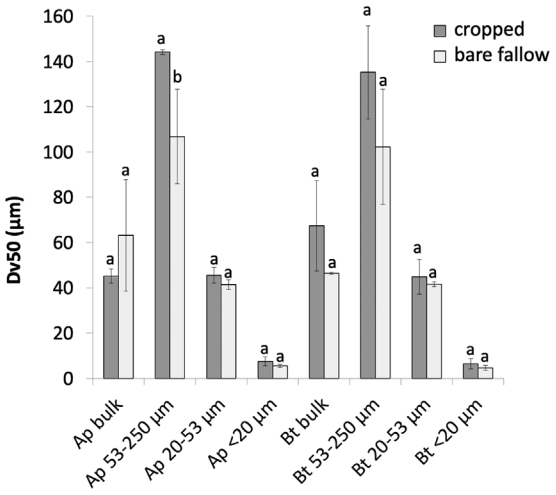

FIGURE 1 Median diameter (Dv50) of bulk soil and size fractions (20–53, <20 µm) for the cropped site and bare fallow for the topsoil (Ap) and subsoil (Bt) horizons. Mean values ± SD, $n = 3$. Lowercase letters indicate significant differences between the treatments but within size fractions ($p < 0.05$).

3.3 | Elemental composition

Considering the bulk soil and the size fractions (20–53 and <20 µm), the OC and N content was mostly significantly higher in the Ap horizon than in the Bt (Table 1). Between the treatments, there were no significant differences between the cropped and the bare fallow for the bulk soil. Treatment effects only became apparent in size- and

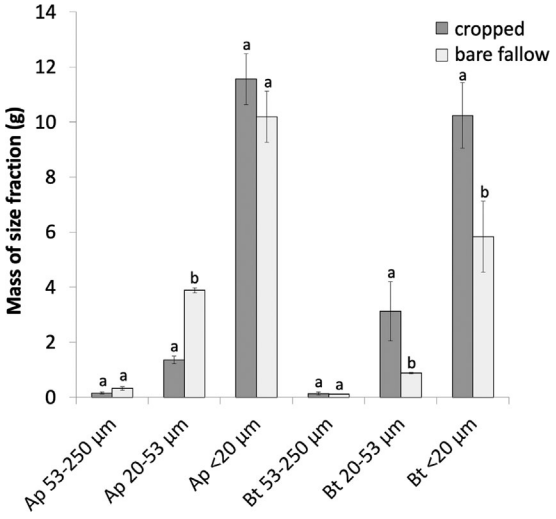

FIGURE 2 Mass distribution of size fractions (53–250, 20–53, <20 µm) for the cropped site and bare fallow for the topsoil (Ap) and subsoil (Bt) horizons. The total dry soil weight which the size fractions refer to was 50 ± 1 g. Mean values ± SD, $n = 3$. Lowercase letters indicate significant differences between the treatments but within size fractions ($p < 0.05$).

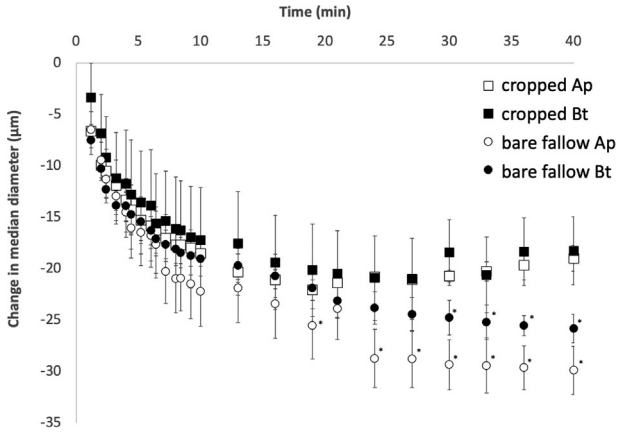

FIGURE 3 Changes in the median diameter (Dv50) of the bulk soil samples from the Ap and Bt horizons for the cropped site and bare fallow during 40 min of continuous measurement of the particle size distribution ($n = 3$). Significant differences within the soil horizon (Ap and Bt) but between treatments (cropped and bare fallow) are denoted with an asterisk ($p < 0.05$).

density-fractionated samples, with an increase of OC in the Bt horizon (only significant for 20–53 and <20 µm and only a trend for <0.30 µm) under bare fallow. Although not significant, there is a trend toward a higher OC content in the Ap horizon for the cropped site. Generally, OC and N tend to accumulate in the <20 µm size fraction, which confirms previous studies showing that OC mainly accumulates in the smallest fractions with the largest specific surface area (Kahle et al., 2002; Krause et al., 2018). The C/N ratio was generally wider in the Ap horizon than in the Bt horizon in all samples. When comparing the size fractions (except <0.30 µm), the C/N ratio was wider in the 20–53 µm size fraction and narrower in the <20 µm size fraction. OM depletion tends to widen the C/N ratio for the 20–53 µm size fraction, while it did not have a clear effect on the bulk soil and the <20 µm size fraction (Table 1).

When considering the total Si, Fe, and Al content, Si did not show a specific trend except for exhibiting a significantly higher content in the samples of the cropped site, compared to bare fallow for the 20–53 µm size fraction, and a significantly higher content in Bt for bare fallow, compared to the Bt of the cropped site (Table 1). This was different for Fe and Al, which tended to have higher content in bare fallow samples, compared to the cropped site, and Bt, compared to Ap in the bulk soil, the <20 µm, and the <0.30 µm size fraction (not all significant). In contrast, in the 20–53 µm size fraction, the content of Fe and Al was higher in the Ap horizon, compared to the Bt horizon (Table 1).

3.4 | ^{14}C content

The size fraction 20–53 µm exhibited the highest ^{14}C content, followed by the bulk soil, while the ^{14}C content was lowest in the <20 µm size fraction (Figure 4; Table S2). Samples from the cropped site always exhibited a higher ^{14}C content than samples from the bare fallow site

TABLE 1 Total elemental composition of bulk soil and size fractions (20–53, <20, <0.30 µm) for the cropped site and bare fallow for the topsoil (Ap) and subsoil horizon (Bt).

Sample	Size (µm)	OC	N	C/N	Si	Fe	Al	Ca
		(%)		(–)	(g kg^{-1})		(mg kg^{-1})	
Cropped Ap	Bulk	1.00 ± 0.06 ^{a}	0.13 ± 0.01 ^{a}	7.7	326 ± 4 ^{a}	18,613 ± 140 ^{a}	36,466 ± 466 ^{a}	3426 ± 30 ^{a}
Cropped Bt	Bulk	0.36 ± 0.05 ^{b}	0.08 ± 0.02 ^{b}	4.5	366 ± 1 ^{b}	20,400 ± 140 ^{b}	42,056 ± 160 ^{b}	3343 ± 26 ^{a}
Bare fallow Ap	Bulk	1.01 ± 0.17 ^{a}	0.13 ± 0.01 ^{a}	7.8	359 ± 2 ^{b}	22,100 ± 300 ^{c}	39,866 ± 400 ^{c}	3683 ± 50 ^{b}
Bare fallow Bt	Bulk	0.33 ± 0.03 ^{b}	0.07 ± 0.01 ^{b}	4.7	296 ± 5 ^{c}	25,200 ± 566 ^{d}	43,216 ± 900 ^{b}	2870 ± 66 ^{c}
Cropped Ap	20–53	0.41 ± 0.03 ^{a}	0.05 ± 0.00 ^{a}	8.5	269 ± 1 ^{a}	4916 ± 73 ^{a}	71,533 ± 633 ^{a}	423 ± 20 ^{a}
Cropped Bt	20–53	0.15 ± 0.01 ^{b}	0.04 ± 0.01 ^{a}	3.8	270 ± 6 ^{a}	1806 ± 36 ^{b}	33,280 ± 1046 ^{b}	606 ± 30 ^{b}
Bare fallow Ap	20–53	0.35 ± 0.02 ^{a}	0.03 ± 0.00 ^{a}	11.7	327 ± 11 ^{b}	3243 ± 63 ^{c}	46,466 ± 1433 ^{c}	964 ± 25 ^{c}
Bare fallow Bt	20–53	0.35 ± 0.04 ^{a}	0.06 ± 0.01 ^{a}	5.8	321 ± 11 ^{b}	2133 ± 73 ^{d}	47,200 ± 1800 ^{c}	155 ± 5 ^{d}
Cropped Ap	<20	1.76 ± 0.12 ^{a}	0.25 ± 0.03 ^{a}	7.0	294 ± 9 ^{a}	19,166 ± 800 ^{a}	36,600 ± 1433 ^{a}	523 ± 40 ^{a}
Cropped Bt	<20	0.59 ± 0.05 ^{b}	0.15 ± 0.00 ^{b}	3.9	338 ± 5 ^{b}	25,003 ± 153 ^{b}	52,533 ± 833 ^{b}	737 ± 11 ^{b}
Bare fallow Ap	<20	1.55 ± 0.28 ^{a}	0.22 ± 0.06 ^{a}	7.0	304 ± 9 ^{ac}	25,066 ± 333 ^{b}	47,733 ± 1366 ^{c}	1307 ± 14 ^{c}
Bare fallow Bt	<20	0.87 ± 0.04 ^{c}	0.21 ± 0.00 ^{a}	4.1	319 ± 7 ^{bc}	36,333 ± 533 ^{c}	63,733 ± 733 ^{d}	1003 ± 30 ^{d}
		(mg kg^{-1})						
Cropped Ap	<0.30	308 ± 57 ^{a}	–	–	2175 ± 583 ^{a}	1019 ± 281 ^{a}	1367 ± 389 ^{a}	60 ± 16 ^{a}
Cropped Bt	<0.30	253 ± 17 ^{a}	–	–	2805 ± 197 ^{a}	1393 ± 89 ^{a}	1736 ± 115 ^{a}	73 ± 7 ^{a}
Bare fallow Ap	<0.30	283 ± 55 ^{a}	–	–	3296 ± 649 ^{ab}	1493 ± 345 ^{a}	2051 ± 450 ^{a}	88 ± 28 ^{a}
Bare fallow Bt	<0.30	317 ± 88 ^{a}	–	–	6137 ± 702 ^{b}	2993 ± 374 ^{b}	3596 ± 444 ^{b}	219 ± 26 ^{b}

Note: Mean values ± SD, $n = 3$. Lowercase letters indicate significant differences between the treatments and horizons but within size fractions ($p < 0.05$).
Abbreviations: C/N, Carbon/nitrogen; Ca, calcium; Fe, iron; OC, organic carbon detector; Si, silicon.

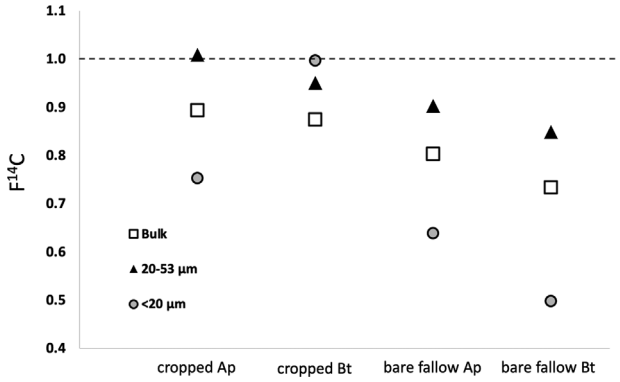

FIGURE 4 ^{14}Carbon (^{14}C) fraction of modern C ($F^{14}C$; ^{14}C content expressed as fraction modern C) value for the cropped site and bare fallow in Ap and Bt horizons, and three size fractions, that is, bulk, 20–53 µm, and <20 µm. The dashed line represents the atmospheric content. Composite samples (weight basis) of three replicates were analyzed.

within the respective soil horizon, and the ^{14}C content in the Bt horizon was lower than in the Ap horizon. The only exception was the ^{14}C content of the <20 µm sample obtained from the Bt of the cropped site, which did not follow any of these trends.

3.5 | Chemical form of Fe

3.5.1 | Oxalate and DCB Fe

The oxalate extraction method involves complexing Fe with oxalate ligands to solubilize the Fe (oxyhydr)oxides, although the quantitative assignment of dissolved Fe to specific minerals like short-range-ordered ferrihydrite is challenging due to the presence of various pedogenic species and the operational nature of the technique (Rennert, 2018; Schwertmann, 1964). When using oxalate extraction in soil analysis, it is important to consider that elements can be released from non-target minerals, especially in impure mineral concentrates or natural clay-mineral samples (Rennert, 2018; Rennert et al., 2021). In particular, adsorbed SOM and allophane can protect Fe (oxyhdr)oxides from ligand-induced and reductive dissolution and influence their solubility (Filimonova et al., 2016; Poggenburg et al., 2018). As the soil did not contain allophanes (C. Jiang et al., 2014), we do not assume an incomplete extraction. However, a bias associated with the adsorption of SOM to ferrihydrite cannot be ruled out here, and therefore the extraction of short-range-ordered Fe (oxyhydr)oxides might be incomplete using oxalate. For the sake of simplicity, however, we will refer to the DCB extractable Fe as total Fe (oxyhydr)oxides and the Fe_{OX} as short-range-ordered Fe in the following and discuss the weaknesses of both methods in more detail where appropriate.

For the bulk soil, we found a significantly lower Fe_{OX} content and a significantly higher Fe_{DCB}-Fe_{OX} content under bare fallow than for the cropped site (Table 2). In the specific size fractions, Fe_{OX} is lower in Bt than in Ap horizons. The content of crystalline Fe oxide (Fe_{DCB}-Fe_{OX}) was lower in Bt than in Ap, while it was higher in Bt under bare fallow, compared to the cropped site. The ratio of Fe_{OX}/Fe_{DCB} is indicative of the contribution of short-range-ordered Fe oxide phases to total Fe oxides. In all samples, the content of both Fe_{OX} and Fe_{DCB} increased with decreasing particle size, maintaining a comparable Fe_{OX}/Fe_{DCB} ratio across the three size separates (Table 2). The only exception to this is the ratio for the Bt 20–53 µm of the cropped site (higher) and bare fallow Bt <20 µm (lower). The ratio is a measure for the proportion of poorly crystalline oxides (Fe_{OX}) within total Fe oxides (Fe_{DCB}).

TABLE 2 Oxalate and dithionite-citrate-bicarbonate iron (Fe_{OX} and Fe_{DCB}) of bulk soil and size fractions (20–53, <20 µm) for the cropped site and bare fallow for the topsoil (Ap) and subsoil (Bt) horizons.

Sample	Size (µm)	Fe_{OX} (g kg^{-1})	Fe_{DCB}	Fe_{DCB-OX}	Fe_{OX}/Fe_{DCB} (–)
Cropped Ap	Bulk	2.53 ± 0.04 [a]	6.33 ± 0.07 [a]	3.80 ± 0.43 [a]	0.40 ± 0.01 [a]
Cropped Bt	Bulk	2.81 ± 0.10 [a]	6.23 ± 0.54 [a]	3.42 ± 0.54 [a]	0.45 ± 0.04 [a]
Bare fallow Ap	Bulk	2.37 ± 0.04 [b]	7.38 ± 0.05 [b]	5.01 ± 0.30 [b]	0.32 ± 0.00 [b]
Bare fallow Bt	Bulk	1.72 ± 0.05 [b]	9.34 ± 0.82 [c]	7.62 ± 0.22 [c]	0.18 ± 0.01 [c]
Cropped Ap	20–53	0.72	1.48	0.76	0.49
Cropped Bt	20–53	0.29	0.39	0.08	0.78
Bare fallow Ap	20–53	0.47	1.11	0.65	0.42
Bare fallow Bt	20–53	0.28	0.69	0.40	0.41
Cropped Ap	<20	3.96	7.74	3.78	0.51
Cropped Bt	<20	3.09	6.00	2.91	0.51
Bare fallow Ap	<20	3.68	8.50	4.83	0.43
Bare fallow Bt	<20	2.59	11.73	9.14	0.22

Note: Mean values ± SD for the bulk soil, $n = 3$. The sample amount was too low for size fractions, meaning that replicates were combined to obtain a composite sample (weight basis), and no replicates could be measured. Lowercase letters indicate significant differences between the treatments and horizons but within bulk soil ($p < 0.05$).
Abbreviations: Fe_{DCB}, dithionite-citrate-bicarbonate extractable Fe; Fe_{OX}, oxalate extractable Fe.

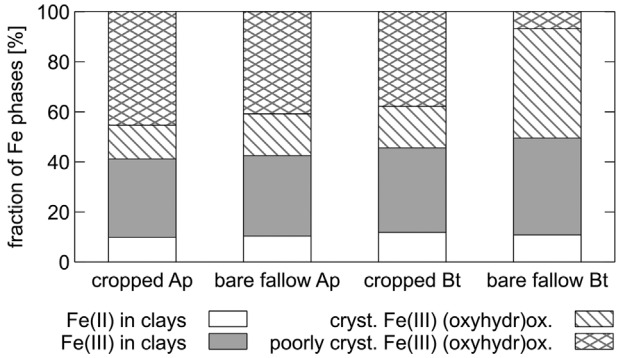

FIGURE 5 Iron (Fe) mineralogy as obtained by Mössbauer spectroscopy for the size fraction <20 μm for the cropped site and bare fallow for the topsoil (Ap) and subsoil (Bt) horizons. The relative fractions of Fe phases shown (Fe(II), Fe(III), crystalline Fe(III) (oxyhydr)oxides, and poorly crystalline Fe(III) (oxyhydr)oxides) are based on measurements at 5 K but the interpretation is based on both measurements at 77 and 5 K. Replicates were combined to obtain a composite sample (weight basis).

3.5.2 | Mössbauer spectroscopy

We used Mössbauer spectroscopy to determine the Fe speciation and mineralogy in different horizons and treatments within the <20 μm aggregate fraction. All collected spectra indicated a constant Fe redox speciation irrespective of horizon or treatment, with 88%–90% Fe(III) and 10%–12% Fe(II) (Figure 5). The Fe(II) was likely bound as Fe(II) in clay minerals and not adsorbed Fe(II) since the analyzed soils are oxic. Overall, we found that 31%–39% of Fe(III) was bound in clay minerals, 14%–44% of crystalline Fe(III) (oxyhydr)oxides, and 7%–45% of poorly crystalline Fe(III) (oxyhydr)oxides. The poorly crystalline phases are expected to contain ferrihydrite, lepidocrocite, and akageneite, and the crystalline phases are expected to comprise goethite and hematite. Note here that we did not assign individual mineral phases because the parameters for the individual phases can vary depending on the OM content, particle size, and structural substitution (Eusterhues et al., 2008; Latta et al., 2012; Murad & Cashion, 2011). The poorly crystalline Fe(III) (oxyhydr)oxide phases mentioned here may also contain ferric (oxyhydr)oxide minerals that have formed in the presence of OM at C/Fe ratios ≤1.5, sometimes referred to as Fe–OM or Fe–OM coprecipitates (Eusterhues et al., 2008; ThomasArrigo et al., 2018).

There were major differences in the abundances of crystalline and poorly crystalline Fe(III) (oxyhydr)oxides based on the treatment. In bare fallow samples, abundances of poorly crystalline Fe(III) (oxyhydr)oxides were lower in both the Ap (41%) and Bt (7%) horizons, compared to the cropped site (Ap: 45%, Bt: 38%). Conversely, abundances of crystalline Fe(III) (oxyhydr)oxides were slightly higher under bare fallow than for the cropped site in both horizons: 17%, compared to 14% in the Ap horizon, and 44%, compared to 38% in the Bt horizon. Differences between the horizons mostly showed a higher abundance of crystalline Fe(III) (oxyhydr)oxides in the Bt horizon than in the Ap horizon (Figure 5).

4 | DISCUSSIONS

4.1 | Bare fallow reduces aggregate stability

Bare fallow led to the destabilization and disintegration of soil microaggregates in both Ap and Bt. In particular, large microaggregates of the Ap (53–250 μm; Figure 1) were disintegrated into small soil microaggregates (20–53 μm), which was confirmed by a significant increase in the mass of small soil microaggregates (Figure 2). The disintegration of large soil microaggregates is a result of the missing input of fresh OM acting as a gluing agent. At higher hierarchy levels, fresh and plant-based OM acts as a temporary gluing agent that glues smaller microaggregates into larger units (Totsche et al., 2018) and is particularly enriched in the Ap horizon. Over time, these gluing agents are decomposed and aggregates disintegrate into smaller units. These significant effects of bare fallow on soil aggregate masses are surprising when considering the different soil management practices of the two sites. While the cropped site is regularly tilled, the Ap of the bare fallow site was left fallow without soil tillage for the last few years (L. Weihermüller & N. Meyer, personal communication, December 01, 2022). Periodic tillage, however, is known to decrease aggregate stability in the Ap horizon caused by different breakdown mechanisms (Six et al., 1998). Therefore, the effect of bare fallow on soil aggregate disintegration is assumed to be greater than what is reflected in the data when compared with the regularly tilled cropped site.

It is known that occluded OM significantly contributes to the stabilization of soil aggregates (Golchin et al., 1994). While in the literature there are contrasting findings on soil aggregate stability with OM content along a soil profile (Bronick & Lal, 2005; Jakšík et al., 2015; Kodešová et al., 2009), we found a decreased stability of aggregates under bare fallow, compared to the cropped site, and in the Ap, compared to the Bt horizon (Figure 3). There are several reasons associated with the aggregate stability with depth in the soil profile, for example, the configuration of clay particles, Fe and Al (hydr)oxide content, OM content, the presence of OM coatings, and porosity (Ellerbrock & Gerke, 2004; Gerke & Köhne, 2002; Kodešová et al., 2009; Roosch et al., 2024). While treatment (cropped vs. bare fallow) did not significantly affect the OC content in the bulk soil, in the size fractions there was a trend toward lower OC content under bare fallow in the Ap horizon (Table 1). With decreasing size fraction, the C/N ratio also decreases (Table 1), suggesting a progressive level of OM decomposition and an increasing contribution of microbial-derived OM (Kahle et al., 2002; Paul, 2016; Tang et al., 2022). Therefore, although not reflected by the OC content of the bulk soil, the OC content decreased in specific size fractions under bare fallow, leading to reduced stability of the aggregates. This also agrees with the findings of Schweizer et al. (2024) on the same site, who suggest that the higher dispersibility of the aggregates at a constant OC content is an effect of the changing gluing properties of the aggregates under bare fallow.

However, it is not only the OC content that plays an important role in the stabilization of aggregates but also pedogenic oxides such as Fe (oxyhydr)oxides acting as cementing agents and fillings within pores (Krause et al., 2020; Totsche et al., 2018). In particular, Fe minerals

with poor crystallinity have high cation and anion exchange capacities and extensive variable-charged surfaces contribute to the formation of predominantly small aggregates with very high stability (Asano et al., 2018; Tisdall & Oades, 1982). This increasing stability with an increasing content of SRO mineral phases explains the smaller changes in median diameter for the cropped site, compared to the bare fallow site (Figure 3). The content of SRO mineral phases was higher for the cropped site than for bare fallow, especially for smaller size fractions (Table 2, Figure 5). Note that the short-range ordered mineral phases may also contain Fe-OM coprecipitates; as the binding environment of Fe atoms is similar to that in ferrihydrite, these phases are indistinguishable from ferrihydrite, especially in natural environments such as soils. This also reaffirms the validity of oxalate extraction, as OC tended to have a higher content for the cropped site, increasing the likelihood of SOM–Fe associations reducing the extractability of oxalate. Since the bulk of the sample consists of aggregates <20 µm (Figure 2) and due to the higher OC content, compared to larger size fractions, the crystallization of SRO mineral phases might have been prevented (Cornell & Schwertmann, 1979; Vodyanitskii & Shoba, 2016), which explains the higher content for the cropped site.

Besides the differences in the content of OM and Fe (oxyhydr)oxide, the water stability of macroaggregates was higher for the cropped site, which was likely due to several factors such as OC and higher connectivity of pores to the external aggregate (Roosch et al., 2024). Additionally, the swelling of clay in the Bt horizon of the bare fallow plot may also have been a factor for the reduced water stability since the clay content in this horizon was higher than in the Ap horizon (Roosch et al., 2024).

4.2 | Role of Fe (oxyhydr)oxides in stabilizing SOM

Although all radiocarbon data are based on only one analysis of a composite sample of all replicates, the higher $F^{14}C$ values for the cropped site, compared to the bare fallow site (bulk soil and size fractions; Figure 4), indicate that the contribution of fresher, plant-derived OC is higher at this site, while the missing input of plants and plant residues at the bare fallow site since 2005 resulted in a lower ^{14}C content. While there is mostly a mixture of young and old C in soil aggregates, the largest size fraction (20–53 µm) of the Ap horizon resembled $F^{14}C$ values of a modern atmospheric ^{14}C level, indicating the presence of less decomposed plant-derived OM, that is, young OC. At the bare fallow site, however, the OC seemingly contains higher proportions of older OC compared to the cropped site (830—5592 years vs. modern—2293 years for bare fallow and cropped, respectively; Table S2). These trends cannot be statistically verified due to missing replicates. However, the trends agree with the X-ray photoelectron spectroscopy findings of Fechner et al. (2023) with more oxidized and N-rich OM compounds under bare fallow, compared to the cropped site. This suggests a higher degree of decomposition of OM. The decreasing ^{14}C content with soil depth is in line with previous studies (Herre et al., 2022; Marschner et al., 2008; Moni et al., 2010; Rethemeyer et al., 2005), which is explained by a lower plant input and longer OC turnover times due to SOM stabilization in deeper soil layers (Fontaine et al., 2007; Paul et al., 1997; Rumpel et al., 2002). There are two mechanisms that explain the stabilization of SOM in relation to Fe (oxyhydr)oxides: (1) the occlusion of the SOM within stable aggregates being thus protected against turnover (e.g., Goebel et al., 2005; Moni et al., 2010) or (2) the preferential adsorption of dissolved SOM onto reactive surface zones (e.g., Asano et al., 2018; K. Kaiser & Guggenberger, 2003; Moni et al., 2010). In this study, the decreasing ^{14}C content with decreasing aggregate size might be a result of aggregate stabilization by Fe_{OX} (higher in smaller size fractions; Table 2, Figure 5) and thus the protection of SOM turnover due to occlusion (Eusterhues et al., 2005; Giannetta et al., 2022; Kleber et al., 2005; Moni et al., 2010; Wagai et al., 2018). However, Fe (oxyhydr)oxides of poor crystallinity are particularly prone to releasing associated OM during anaerobic Fe reduction events, which may in turn result in a higher turnover of the associated OM, compared to OM associated with more crystalline Fe (oxyhydr)oxides. This might also explain our results that under bare fallow, older C (i.e., slower cycling SOM with a lower $F^{14}C$ content) is associated with more crystalline Fe phases as was also observed by Hall et al. (2018).

Under bare fallow, the ^{14}C content is also higher than for the cropped site (Figure 3), which can be attributed to the lack of input of fresh OM by plants. However, it is surprising that this effect is quite pronounced not only in the topsoil but also in the subsoil. In more than half of Germany's arable soils, the potential rooting was restricted mainly due to the compactness of the soil (Schneider & Don, 2019). The input of fresh SOM in the form of plant roots in the subsoil is thus also lower, and the effects of bare fallow should therefore not be as pronounced. A possible explanation for this might be the translocation of SOM from the topsoil into the subsoil by soil colloids. While the dominant soil-forming process in Luvisols is the translocation of clay-sized mineral particles from the A to the Bt horizon, results of this study indicated that colloids are formed that are additionally transported from the subsoil into deeper soil layers due to the disintegration of aggregates under bare fallow. Mobile soil colloids in arable soil are generally composed of associations of nanosized OC, clay minerals, and Fe/Al (oxyhydr)oxides (X. Jiang et al., 2015; Siebers et al., 2023; Tang et al., 2022) and can be transported below ground (Fresne et al., 2022). However, nano colloids up to 20 nm are particularly highly mobile in soil (Siebers et al., 2023) and are mainly composed of OC in arable soils (X. Jiang et al., 2015; Krause et al., 2020; Siebers et al., 2023). The breakdown of aggregates under bare fallow releases mobile colloids. Studies have shown that SOM that is occluded and associated with small-size fractions has a higher degree of decomposition and higher turnover times. It can therefore be considered older (Tang et al., 2022; Totsche et al., 2018; Wagai et al., 2018). Although not measured in this study, we assume that older SOM was predominantly transported with the released colloids, as was also found for other soils (Tang et al., 2022). Due to their mobility, these colloids were transported into the subsoil, which was confirmed by a significant increase of OC, Fe, Al, and Si (only in colloidal size fraction <0.30 µm) in the Bt horizon (Table 1). The Si in colloids predominantly originated from clay minerals, which are potentially mobile due to their small size, whereas the Si in larger size fractions may also originate from primary particles with lower mobility.

5 | CONCLUSION

As hypothesized, there is a relationship between the turnover and composition of OM in aggregates and the chemical form of Fe. We were able to demonstrate that (1) bare fallow led to the destabilization of large soil microaggregates and their subsequent decomposition into small soil microaggregates, thus increasing the mass of small aggregates. This effect was more pronounced in the Ap horizon and (2) was attributed to a decrease in C content and (3) a decrease in poorly crystalline Fe minerals. The ^{14}C content decreased with decreasing size fraction, suggesting greater stability and longer turnover times for SOM, especially in deeper soil layers. Turnover times are closely related to different Fe phases that are associated with different SOM pools. Therefore, the stability and abundance of larger microaggregates seem to be directly linked to the availability of fresh OM. In turn, the stability of small microaggregates appears to be due to mineral phases, in particular of poorly crystalline Fe (oxyhydr)oxides. Despite being stable and enriched in Fe (oxyhydr)oxides, the small-sized microaggregates had the largest losses of younger C, indicating the preferential protection of older OM. The destabilization of soil aggregates under bare fallow led to the formation of mobile soil nanocolloids. The transport of colloids and associated elements can initiate elemental fluxes with as-yet-unknown consequences for nutrient losses from ecosystems and associated environmental risks. In general, OM depletion due to continuous bare fallow likely induced an overall transition of soil architecture to a new steady state. This has consequences for OM storage and stabilization but likely also for soil physical properties.

ACKNOWLEDGMENTS

This work was undertaken within the *MAD Soil project* (*MAD Soil—Microaggregates: Formation and turnover of the structural building blocks of soils*), which is funded by the *German Research Foundation* (*DFG, research unit 2179*). We would like to thank *Fabian Kuhlen* for performing the DCB and oxalate extraction and analyses, *Ni Tang* for assisting with size and density fractionation, *Roland Bol* for his advice on the ^{14}C measurements, and *Erwin Klumpp* for his discussions. We would also like to give special thanks to *P. Narf* for his constructive suggestions during the writing process.

Open access funding enabled and organized by Projekt DEAL.

DATA AVAILABILITY STATEMENT

The data that support the findings of this study are available from the corresponding author upon reasonable request.

ORCID

Nina Siebers https://orcid.org/0000-0002-6431-0046
Eva Voggenreiter https://orcid.org/0000-0001-7996-9129

REFERENCES

Amézketa, E. (1999). Soil aggregate stability: A review. *Journal of Sustainable Agriculture*, *14*(2-3), 83–151.

Asano, M., Wagai, R., Yamaguchi, N., Takeichi, Y., Maeda, M., Suga, H., & Takahashi, Y. (2018). In search of a binding agent: Nano-scale evidence of preferential carbon associations with poorly-crystalline mineral phases in physically-stable, clay-sized aggregates. *Soil Systems*, *2*(2), 32. https://doi.org/10.3390/soilsystems2020032

Barberis, E., Marsan, F. A., Boero, V., & Arduino, E. (1991). Aggregation of soil particles by iron oxides in various size fractions of soil B horizons. *Journal of Soil Science*, *42*(4), 535–542.

Bauke, S. L., Amelung, W., Bol, R., Brandt, L., Brüggemann, N., Kandeler, E., Meyer, N., Or, D., Schnepf, A., Schloter, M., Schulz, S., Siebers, N., von Sperbe, C., & Vereecken, H. (2022). Soil water status shapes nutrient cycling in agroecosystems from micrometer to landscape scales. *Journal of Plant Nutrition and Soil Science*, *185*(6), 773–792.

Bronick, C. J., & Lal, R. (2005). Soil structure and management: A review. *Geoderma*, *124*(1-2), 3–22.

Chen, C., Kukkadapu, R., & Sparks, D. L. (2015). Influence of coprecipitated organic matter on Fe^{2+} (aq)-catalyzed transformation of ferrihydrite: Implications for carbon dynamics. *Environmental Science & Technology*, *49*(18), 10927–10936.

Cornell, R. M., & Schwertmann, U. (1979). Influence of organic anions on the crystallization of ferrihydrite. *Clays and Clay Minerals*, *27*(6), 402–410.

Cornell, R. M., & Schwertmann, U. (2003). *The iron oxides: Structure, properties, reactions, occurrences, and uses*. Wiley-VCH.

Ellerbrock, R. H., & Gerke, H. H. (2004). Characterizing organic matter of soil aggregate coatings and biopores by Fourier transform infrared spectroscopy. *European Journal of Soil Science*, *55*(2), 219–228.

Eusterhues, K., Rumpel, C., Kleber, M., & Kögel-Knabner, I. (2003). Stabilisation of soil organic matter by interactions with minerals as revealed by mineral dissolution and oxidative degradation. *Organic Geochemistry*, *34*(12), 1591–1600.

Eusterhues, K., Rumpel, C., & Kögel-Knabner, I. (2005). Organo-mineral associations in sandy acid forest soils: Importance of specific surface area, iron oxides and micropores. *European Journal of Soil Science*, *56*(6), 753–763.

Eusterhues, K., Wagner, F. E., Häusler, W., Hanzlik, M., Knicker, H., Totsche, K. U., Kögel-Knabner, I., & Schwertmann, U. (2008). Characterization of ferrihydrite-soil organic matter coprecipitates by X-ray diffraction and Mossbauer spectroscopy. *Environmental Science & Technology*, *42*(21), 7891–7897.

Fechner, A., Mikutta, R., Kaiser, K., Bromm, T., Vogel, C., Zethof, J., Aehnelt, M., Guggenberger, G., & Dultz, S., (2023). Changes in soil organic matter quality during long-term bare fallow do not affect microaggregate stability. *EGU General Assembly 2023*, Vienna, Austria, 24–28 Apr 2023, EGU23-15453. https://doi.org/10.5194/egusphere-egu23-15453, 2023

Filimonova, S., Kaufhold, S., Wagner, F. E., Häusler, W., & Kögel-Knabner, I. (2016). The role of allophane nano-structure and Fe oxide speciation for hosting soil organic matter in an allophanic Andosol. *Geochimica et Cosmochimica Acta*, *180*, 284–302.

Fontaine, S., Barot, S., Barré, P., Bdioui, N., Mary, B., & Rumpel, C. (2007). Stability of organic carbon in deep soil layers controlled by fresh carbon supply. *Nature*, *450*(7167), 277–280.

Fresne, M., Jordan, P., Daly, K., Fenton, O., & Mellander, P. E. (2022). The role of colloids and other fractions in the below-ground delivery of phosphorus from agricultural hillslopes to streams. *Catena*, *208*, 105735. https://doi.org/10.1016/j.catena.2021.105735

Gerke, H. H., & Köhne, J. M. (2002). Estimating hydraulic properties of soil aggregate skins from sorptivity and water retention. *Soil Science Society of America Journal*, *66*(1), 26–36.

Giannetta, B., Plaza, C., Thompson, A., Plante, A. F., & Zaccone, C. (2022). Iron speciation in soil size fractions under different land uses. *Geoderma*, *418*, 115842. https://doi.org/10.1016/j.geoderma.2022.115842

Goebel, M. O., Bachmann, J., Woche, S. K., & Fischer, W. R. (2005). Soil wettability, aggregate stability, and the decomposition of soil organic matter. *Geoderma*, *128*(1-2), 80–93.

Golchin, A., Oades, J. M., Skjemstad, J. O., & Clarke, P. (1994). Soil structure and carbon cycling. *Soil Research*, *32*(5), 1043–1068.

Hall, S. J., Berhe, A. A., & Thompson, A. (2018). Order from disorder: Do soil organic matter composition and turnover co-vary with iron phase crystallinity? *Biogeochemistry*, *140*, 93–110.

Herre, M., Heitkötter, J., Heinze, S., Rethemeyer, J., Preusser, S., Kandeler, E., & Marschner, B. (2022). Differences in organic matter properties and microbial activity between bulk and rhizosphere soil from the top-and subsoils of three forest stands. *Geoderma*, *409*, 115589. https://doi.org/10.1016/j.geoderma.2021.115589

ISO. (1995). ISO *10694: Determination of organic and total carbon after dry combustion (elementary analysis)*. AFNOR. https://www.iso.org/standard/18782.html#:~:text=Specifies%20a%20method%20for%20the,carbon%20content%20is%20measured%20directly

Jakšík, O., Kodešová, R., Kubiš, A., Stehlíková, I., Drábek, O., & Kapička, A. (2015). Soil aggregate stability within morphologically diverse areas. *Catena*, *127*, 287–299.

Jiang, C., Séquaris, J. M., Wacha, A., Bóta, A., Vereecken, H., & Klumpp, E. (2014). Effect of metal oxide on surface area and pore size of water-dispersible colloids from three German silt loam topsoils. *Geoderma*, *235*, 260–270.

Jiang, X., Bol, R., Nischwitz, V., Siebers, N., Willbold, S., Vereecken, H., Amelung, W., & Klumpp, E. (2015). Phosphorus containing water dispersible nanoparticles in arable soil. *Journal of Environmental Quality*, *44*(6), 1772–1781.

Jones, A. M., Collins, R. N., Rose, J., & Waite, T. D. (2009). The effect of silica and natural organic matter on the Fe (II)-catalysed transformation and reactivity of Fe (III) minerals. *Geochimica et Cosmochimica Acta*, *73*(15), 4409–4422.

Kahle, M., Kleber, M., & Jahn, R. (2002). Carbon storage in loess derived surface soils from Central Germany: Influence of mineral phase variables. *Journal of Plant Nutrition and Soil Science*, *165*(2), 141–149.

Kaiser, K., & Guggenberger, G. (2000). The role of DOM sorption to mineral surfaces in the preservation of organic matter in soils. *Organic Geochemistry*, *31*(7–8), 711–725.

Kaiser, K., & Guggenberger, G. (2003). Mineral surfaces and soil organic matter. *European Journal of Soil Science*, *54*(2), 219–236.

Kaiser, M., & Berhe, A. A. (2014). How does sonication affect the mineral and organic constituents of soil aggregates?—A review. *Journal of Plant Nutrition and Soil Science*, *177*(4), 479–495.

Kaiser, M., Berhe, A. A., Sommer, M., & Kleber, M. (2012). Application of ultrasound to disperse soil aggregates of high mechanical stability. *Journal of Plant Nutrition and Soil Science*, *175*(4), 521–526.

Kiem, R., & Kögel-Knabner, I. (2002). Refractory organic carbon in particle-size fractions of arable soils II: Organic carbon in relation to mineral surface area and iron oxides in fractions < 6 µm. *Organic Geochemistry*, *33*(12), 1699–1713.

Kleber, M., Mikutta, R., Torn, M. S., & Jahn, R. (2005). Poorly crystalline mineral phases protect organic matter in acid subsoil horizons. *European Journal of Soil Science*, *56*(6), 717–725.

Kodešová, R., Rohošková, M., & Žigová, A. (2009). Comparison of aggregate stability within six soil profiles under conventional tillage using various laboratory tests. *Biologia*, *64*, 550–554.

Kögel-Knabner, I., Guggenberger, G., Kleber, M., Kandeler, E., Kalbitz, K., Scheu, S., Eusterhues, K., & Leinweber, P. (2008). Organo-mineral associations in temperate soils: Integrating biology, mineralogy, and organic matter chemistry. *Journal of Plant Nutrition and Soil Science*, *171*(1), 61–82.

Krause, L., Klumpp, E., Nofz, I., Missong, A., Amelung, W., & Siebers, N. (2020). Colloidal iron and organic carbon control soil aggregate formation and stability in arable Luvisols. *Geoderma*, *374*, 114421.

Krause, L., Rodionov, A., Schweizer, S. A., Siebers, N., Lehndorff, E., Klumpp, E., & Amelung, W. (2018). Microaggregate stability and storage of organic carbon is affected by clay content in arable Luvisols. *Soil and Tillage Research*, *182*, 123–129.

Kretzschmar, R., & Sticher, H. (1997). Transport of humic-coated iron oxide colloids in a sandy soil: Influence of Ca^{2+} and trace metals. *Environmental Science & Technology*, *31*(12), 3497–3504.

Lagarec, K., & Rancourt, D. G. (1998). *Recoil-Mössbauer spectral analysis software for Windows*. University of Ottawa.

Latta, D. E., Bachman, J. E., & Scherer, M. M. (2012). Fe electron transfer and atom exchange in goethite: Influence of Al-substitution and anion sorption. *Environmental Science & Technology*, *46*(19), 10614–10623.

Lehmann, J., Kinyangi, J., & Solomon, D. (2007). Organic matter stabilization in soil microaggregates: Implications from spatial heterogeneity of organic carbon contents and carbon forms. *Biogeochemistry*, *85*, 45–57.

Lopez-Sangil, L., & Rovira, P. (2013). Sequential chemical extractions of the mineral-associated soil organic matter: An integrated approach for the fractionation of organo-mineral complexes. *Soil Biology and Biochemistry*, *62*, 57–67.

Marschner, B., Brodowski, S., Dreves, A., Gleixner, G., Gude, A., Grootes, P. M., Hamer, U., Heim, A., Jandl, G., Ji, R., Kaiser, K., Kalbitz, K., Kramer, C., Leinweber, P., Rethemeyer, J., Schäffer, A., Schmidt, M. W. I., Schwark, L., & Wiesenberg, G. L. B. (2008). How relevant is recalcitrance for the stabilization of organic matter in soils? *Journal of Plant Nutrition and Soil Science*, *171*(1), 91–110.

Mason, J. A., Greene, R. S., & Joeckel, R. M. (2011). Laser diffraction analysis of the disintegration of aeolian sedimentary aggregates in water. *Catena*, *87*(1), 107–118.

Meyer, N., Bornemann, L., Welp, G., Schiedung, H., Herbst, M., & Amelung, W. (2017). Carbon saturation drives spatial patterns of soil organic matter losses under long-term bare fallow. *Geoderma*, *306*, 89–98.

Moni, C., Rumpel, C., Virto, I., Chabbi, A., & Chenu, C. (2010). Relative importance of sorption versus aggregation for organic matter storage in subsoil horizons of two contrasting soils. *European Journal of Soil Science*, *61*(6), 958–969.

Murad, E., & Cashion, J. (2011). *Mössbauer spectroscopy of environmental materials and their industrial utilization*. Springer Science & Business Media.

Nischwitz, V., Gottselig, N., Missong, A., Meyn, T., & Klumpp, E. (2016). Field flow fractionation online with ICP-MS as novel approach for the quantification of fine particulate carbon in stream water samples and soil extracts. *Journal of Analytical Atomic Spectrometry*, *31*(9), 1858–1868.

Paul, E. A. (2016). The nature and dynamics of soil organic matter: Plant inputs, microbial transformations, and organic matter stabilization. *Soil Biology and Biochemistry*, *98*, 109–126.

Paul, E. A., Follett, R. F., Leavitt, S. W., Halvorson, A., Peterson, G. A., & Lyon, D. J. (1997). Radiocarbon dating for determination of soil organic matter pool sizes and dynamics. *Soil Science Society of America Journal*, *61*(4), 1058–1067.

Poggenburg, C., Mikutta, R., Liebmann, P., Koch, M., & Guggenberger, G. (2018). Siderophore-promoted dissolution of ferrihydrite associated with adsorbed and coprecipitated natural organic matter. *Organic Geochemistry*, *125*, 177–188.

Regelink, I. C., Voegelin, A., Weng, L., Koopmans, G. F., & Comans, R. N. (2014). Characterization of colloidal Fe from soils using field-flow fractionation and Fe K-edge X-ray absorption spectroscopy. *Environmental Science & Technology*, *48*(8), 4307–4316.

Reimer, P. J., Brown, T. A., & Reimer, R. W. (2004). Discussion: Reporting and calibration of post-bomb ^{14}C data. *Radiocarbon*, *46*(3), 1299–1304.

Rennert, T. (2018). Wet-chemical extractions to characterise pedogenic Al and Fe species—A critical review. *Soil Research*, *57*(1), 1–16.

Rennert, T., Dietel, J., Heilek, S., Dohrmann, R., & Mansfeldt, T. (2021). Assessing poorly crystalline and mineral-organic species by extracting Al, Fe, Mn, and Si using (citrate-) ascorbate and oxalate. *Geoderma*, *397*, 115095.

Rethemeyer, J., Gierga, M., Heinze, S., Stolz, A., Wotte, A., Wischhöfer, P., Berg, S., Melchert, J. O., & Dewald, A. (2019). Current sample preparation and analytical capabilities of the radiocarbon laboratory at CologneAMS. *Radiocarbon*, *61*(5), 1449–1460.

Rethemeyer, J., Kramer, C., Gleixner, G., John, B., Yamashita, T., Flessa, H., Andersen, N., Nadeau, M.-J., & Grootes, P. M. (2005). Transformation of organic matter in agricultural soils: Radiocarbon concentration versus soil depth. *Geoderma*, *128*(1), 94–105.

Roosch, S., Felde, V. J. M. N. L., Uteau, D., & Peth, S. (2024). Exploring the mechanisms of diverging mechanical and water stability in macro-and microaggregates. *Journal of Plant Nutrition and Soil Science*, *187*, 104–117. https://doi.org/10.1002/jpln.202300245

Rumpel, C., Kögel-Knabner, I., & Bruhn, F. (2002). Vertical distribution, age, and chemical composition of organic carbon in two forest soils of different pedogenesis. *Organic Geochemistry*, *33*(10), 1131–1142.

Schneider, F., & Don, A. (2019). Root-restricting layers in German agricultural soils. Part I: Extent and cause. *Plant and Soil*, *442*, 433–451.

Schweizer, S. A., Aehnelt, M., Bucka, F., Totsche, K. U., & Kögel-Knabner, I. (2024). Impact of bare fallow management on soil carbon storage and aggregates across a rock gradient. *Journal of Plant Nutrition and Soil Science*, *187*, 118–129. https://doi.org/10.1002/jpln.202300156

Schwertmann, U. (1964). Differenzierung der eisenoxide des bodens durch extraktion mit ammoniumoxalat-Lösung. *Zeitschrift für Pflanzenernährung, Düngung, Bodenkunde*, *105*(3), 194–202.

Schwertmann, U., & Carlson, L. (2005). The pH-dependent transformation of schwertmannite to goethite at 25°C. *Clay Minerals*, *40*(1), 63–66.

Siebers, N., Bauke, S. L., Tamburini, F., & Amelung, W. (2018). Short-term impacts of forest clear-cut on P accessibility in soil microaggregates: An oxygen isotope study. *Geoderma*, *315*, 59–64.

Siebers, N., Kruse, J., Jia, Y., Lennartz, B., & Koch, S. (2023). Loss of subsurface particulate and truly dissolved phosphorus during various flow conditions along a tile drain–ditch–brook continuum. *Science of the Total Environment*, *866*, 161439. https://doi.org/10.1016/j.scitotenv.2023.161439

Six, J., Bossuyt, H., Degryze, S., & Denef, K. (2004). A history of research on the link between (micro) aggregates, soil biota, and soil organic matter dynamics. *Soil and Tillage Research*, *79*(1), 7–31.

Six, J., Elliott, E. T., Paustian, K., & Doran, J. W. (1998). Aggregation and soil organic matter accumulation in cultivated and native grassland soils. *Soil Science Society of America Journal*, *62*(5), 1367–1377.

Six, J., Feller, C., Denef, K., Ogle, S., de Moraes Sa, J. C., & Albrecht, A. (2002). Soil organic matter, biota and aggregation in temperate and tropical soils-Effects of no-tillage. *Agronomie*, *22*(7–8), 755–775.

Tang, N., Siebers, N., Leinweber, P., Eckhardt, K. U., Dultz, S., Nischwitz, V., & Klumpp, E. (2022). Implications of free and occluded fine colloids for organic matter preservation in arable soils. *Environmental Science & Technology*, *56*(19), 14133–14145.

ThomasArrigo, L. K., Byrne, J. M., Kappler, A., & Kretzschmar, R. (2018). Impact of organic matter on iron (II)-catalyzed mineral transformations in ferrihydrite–organic matter coprecipitates. *Environmental Science & Technology*, *52*(21), 12316–12326.

Tisdall, J. M., & Oades, J. M. (1982). Organic matter and water-stable aggregates in soils. *Journal of Soil Science*, *33*(2), 141–163.

Tombácz, E., Libor, Z., Illes, E., Majzik, A., & Klumpp, E. (2004). The role of reactive surface sites and complexation by humic acids in the interaction of clay mineral and iron oxide particles. *Organic Geochemistry*, *35*(3), 257–267.

Torn, M. S., Trumbore, S. E., Chadwick, O. A., Vitousek, P. M., & Hendricks, D. M. (1997). Mineral control of soil organic carbon storage and turnover. *Nature*, *389*, 6647. https://doi.org/10.1038/38260

Totsche, K. U., Amelung, W., Gerzabek, M. H., Guggenberger, G., Klumpp, E., Knief, C., Lehndorff, E., Mikutta, R., Peth, S., Prechtel, A., Ray, N., & Kögel-Knabner, I. (2018). Microaggregates in soils. *Journal of Plant Nutrition and Soil Science*, *181*(1), 104–136.

Totsche, K. U., Rennert, T., Gerzabek, M. H., Kögel-Knabner, I., Smalla, K., Spiteller, M., & Vogel, H.-J. (2010). Biogeochemical interfaces in soil: The interdisciplinary challenge for soil science. *Journal of Plant Nutrition and Soil Science*, *173*(1), 88–99.

Virto, I., Barré, P., & Chenu, C. (2008). Microaggregation and organic matter storage at the silt-size scale. *Geoderma*, *146*(1–2), 326–335.

Vodyanitskii, Y. N., & Shoba, S. A. (2016). Ferrihydrite in soils. *Eurasian Soil Science*, *49*, 796–806.

Voelz, J. L., Johnson, N. W., Chun, C. L., Arnold, W. A., & Penn, R. L. (2019). Quantitative dissolution of environmentally accessible iron residing in iron-rich minerals: A review. *ACS Earth and Space Chemistry*, *3*(8), 1371–1392.

Wagai, R., Kajiura, M., Uchida, M., & Asano, M. (2018). Distinctive roles of two aggregate binding agents in allophanic Andisols: Young carbon and poorly-crystalline metal phases with old carbon. *Soil Systems*, *2*(2), 29. https://doi.org/10.3390/soilsystems2020029

Wagai, R., & Mayer, L. M. (2007). Sorptive stabilization of organic matter in soils by hydrous iron oxides. *Geochimica et Cosmochimica Acta*, *71*(1), 25–35.

SUPPORTING INFORMATION

Additional supporting information can be found online in the Supporting Information section at the end of this article.

How to cite this article: Siebers, N., Voggenreiter, E., Joshi, P., Rethemeyer, J., & Wang, L. (2024). Synergistic relationships between the age of soil organic matter, Fe speciation, and aggregate stability in an arable Luvisol. *Journal of Plant Nutrition and Soil Science*, *187*, 77–88. https://doi.org/10.1002/jpln.202300020